Spin-Orbit Torque Switching in a Nearly Compensated Heusler Ferrimagnet

*Joseph Finley[1], Chia-Hao Lee[2], Pinshane Huang[2], and Luqiao Liu[1]**

[1]Department of Electrical Engineering and Computer Science,
Massachusetts Institute of Technology, Cambridge, Massachusetts 02139, USA

[2] Department of Materials Science and Engineering,
University of Illinois Urbana-Champaign, Urbana Illinois 61801, USA

Keywords: spintronics, ferrimagnetic, Heusler alloy, magnetic switching, spin-torque

Ferrimagnetic materials combine the advantages of the low magnetic moment of an antiferromagnet and the easiness of realizing magnetic reading of a ferromagnet. Recently, it was demonstrated that compensated ferrimagnetic half metals can be realized in Heusler alloys, where high spin polarization, zero magnetic moment, and low magnetic damping can be achieved at the same time. In this work, by studying the spin orbit torque induced switching in Heusler alloy $Mn_2Ru_{1-x}Ga$, we found that efficient current-induced magnetic switching can be realized in a nearly compensated sample with strong perpendicular anisotropy and large film thickness. Our work demonstrates the possibility of employing compensated Heusler alloys for fast, energy-efficient spintronic devices.

This is the author manuscript accepted for publication and has undergone full peer review but has not been through the copyediting, typesetting, pagination and proofreading process, which may lead to differences between this version and the Version of Record. Please cite this article as doi: 10.1002/adma.201805361.

Heusler alloys represent a family of promising spintronic materials because of the potential to realize high spin polarization, strong perpendicular anisotropy and low magnetic damping[1–10]. Useful properties such as half metallicity, multiferroicity, compensated magnetization, and non-trivial topological order (i.e. topological insulator) can be precisely engineered with the flexible structure of the Heusler compound [11]. Particularly, following the simple Slater-Pauling rule, one can manipulate the magnetization of Heusler compound by varying the number of valence electrons per unit cell[9,10,12–17]. Recently, by tuning the Ru concentration in a manganese based Heusler alloy $Mn_2Ru_{1-x}Ga$, compensated ferrimagnetic half-metals were realized, where the chemical doping simultaneously adjusted the net magnetic moment to zero and moved the Fermi level into the spin gap [18]. Compensated ferrimagnetic half-metals have the combined advantages of half metallicity and zero net magnetic moment. The gap-opening in one spin sub-band at the Fermi level provides the possibility of reaching high magnetoresistance and low magnetic damping, while the compensated net magnetic moment can lead to high storage density due to the absence of stray field. In contrast to an antiferromagnet, which also has a diminished magnetic moment, compensated ferrimagnets have reduced symmetry and allow for easier magnetic reading and writing. Because of the chemical or crystallographic nonequivalence of the two spin sub-lattices, the magnetic states in compensated ferrimagnets can be detected using standard ferromagnetic measurement techniques, such as tunneling magnetoresistance, anomalous Hall effect, and magneto-optic methods[19–21]. So far, compensated Heusler ferrimagnets have been employed as fixed layers in magnetic devices, where a tunneling magnetoresistance up to 40% and strong perpendicular anisotropy (large exchange bias) have been demonstrated[22–25]. However, the most intriguing application of compensated Heusler alloys, i.e., using them as fast switching magnetic free layers for information storage, remains to be explored. It is an open question whether these zero-moment magnets can be electrically switched. In this work,

we study the Heusler compound $Mn_2Ru_{1-x}Ga$ for its potential usage as a magnetic free layer. We demonstrate that efficient spin-orbit torque induced switching[26] can be realized in a $Mn_2Ru_{1-x}Ga$/Pt bilayer structure with a nearly compensated magnetic moment. The high spin-orbit torque efficiency, ultra-low net magnetization, and the potential to reach low damping and fast switching make these materials ideal candidates for future magnetic memory studies.

The Heusler alloy $Mn_2Ru_{1-x}Ga$ $(0 \leq x \leq 1)$ has two sub-lattices of Mn atoms which occupy crystallographically different sites – 4a site and 4c site as in **Figure 1(a)**. The spins of Mn atoms at these two inequivalent sites couple antiparallel with each other. The $Mn_2Ru_{1-x}Ga$ alloy can be viewed as a mixture of the full Heusler alloy (cubic X_a phase) of Mn_2RuGa which carries 1 μ_B magnetic moment per formula unit (f.u.) and half Heusler (cubic $C1_b$ phase) alloy of Mn_2Ga which has -1 μ_B magnetic moment per f.u. according to the modified Slater-Pauling curve[18,27]. Because the $C1_b$ phase can be generated by removing all Ru atoms from the X_a phase, by varying the Ru concentration 1-x between 0 and 1, one can change the magnetization of the system continuously from -1 μ_B to 1 μ_B per f.u.. Meanwhile, magnetization measurements and first principle calculations suggest that near the compensation point, $Mn_2Ru_{1-x}Ga$ is a half metal with fully polarized conduction electrons[18,27].

To grow $Mn_2Ru_{1-x}Ga$ thin films with the desired phase, we co-sputtered from Mn_2Ga and Ru targets onto MgO (001) substrates, following the results of H. Kurt et al.[18]. For Ru concentration 1-x = 0.4 ~ 1, we find the cubic phase, which is verified by the position of (002) and (004) diffraction peaks in the x-ray diffraction spectrum (**Figure 1(f)**). We further explored the crystal structure of $Mn_2Ru_{1-x}Ga$ films with scanning transmission electron microscopy (STEM). **Figure 1(b)** shows a STEM image from a 100 nm Mn_2Ru_1Ga sample that is capped with a 3 nm Ru protection layer. As seen from the STEM image of the bottom

interface (**Figure 1(e)**), a clear epitaxial relationship exists between the MgO <100> and Mn_2Ru_1Ga <110> planes. Meanwhile, the bulk region of the Mn_2Ru_1Ga film shows a clear alternating contrast between adjacent atomic planes (**Figure 1(c)**) in vertical direction, which is consistent with the crystal structure illustrated in Figure 1(a), because the planes containing Ru atoms appear brighter in the dark field image due to the larger atomic number (Z). The lack of horizontal modulation of contrast might be due to overlapping crystal domains, which leads to intermixing of Ru and Mn atoms in the <110> viewing direction. This out-of-plane ordering also agrees with the XRD data, where a relatively low ratio of the (002) peak versus the (004) peak is obtained in the samples with cubic phase. The signal strength between the two peaks reflects the ordering of the Mn-Ga plane and Mn-Ru plane in $Mn_2Ru_{1-x}Ga$ films. In our experiment, this ratio is smaller than < 2%, indicating a good out-of-plane chemical ordering. Finally, the STEM images show a very smooth surface for the deposited films. The surface morphology is further characterized by AFM, with typical RMS roughness < 0.5 nm (Supporting Information), which provides an ideal platform for future integration with magnetic tunnel junctions.

In order to search for the magnetic compensation point, we carried out magnetometry studies on $Mn_2Ru_{1-x}Ga$ films with $1-x = 0.4 \sim 1$ (**Figure 1(g)**). The dependence of magnetization on the Ru concentration is summarized in **Figure 1(h)**. With additional anomalous Hall effect measurements (Supporting Information), we verified that the magnetization compensation happens between $1-x = 0.78$ and $1-x = 1$. The sign reversal in the anomalous Hall effect signal is a clear evidence for crossover of magnetic moment with zero axis[18,20], as the Hall resistance is dominated by Mn sublattice of site 4a while the net moment is controlled by the competition between the 4a and 4c Mn sublattices[28]. By varying the Ru concentration, the net moment varies because of the hybridization between the orbits

of the 4c Mn and Ru atoms, as well as the change in the total strain in the system[28]. The determined Ru concentration for magnetization compensation (1-$x \approx 0.83$) is slightly higher than previous reports, probably due to the dependence on the crystal strain and ordering[27,29]. In addition to the evolution of the net magnetic moment, we also observe perpendicular magnetic anisotropy in all of the $Mn_2Ru_{1-x}Ga$ samples. This is due to the small (< 2%) lattice mismatch between the substrate and deposited films. From XRD data and STEM studies, we find that the $Mn_2Ru_{1-x}Ga$ films has an out of plane lattice constant of c = 605~608 pm, in contrast to the lattice constant of MgO ($\sqrt{2}a = 596\,pm$), resulting in a small tetragonal distortion and perpendicular magnetic anisotropy.

The threshold current density for spin-torque switching is generally proportional to the free magnetic layer thickness. Therefore, in order to realize practical spin-torque switching, films with low thicknesses are usually required. In previous studies, thick films of $Mn_2Ru_{1-x}Ga$ (thickness > 60 nm) are usually employed for magnetic and electrical properties characterization[18]. To achieve ultrathin Heusler films, we studied the thickness dependence of magnetic properties in $Mn_2Ru_{1-x}Ga$. Here we pick 1-x = 0.68 to reach low net magnetization and a square hysteresis loop (Figure 1(g)). **Figure 2(a)** shows XRD spectra of $Mn_2Ru_{0.68}Ga$ films with different thicknesses. When the film thickness is reduced, the diffraction peak shows a smaller 2θ value, indicating that there is an increase in the *c*-axis lattice parameter, due to the increased strain from the MgO substrate. The effects of this increased tetragonal distortion are also reflected in the M-H curves of **Figure 2(b)**, where the coercivity increases as the film thickness decreases. When the film thickness is less than 11 nm, the (004) diffraction peak is very weak, which might come from the lattice mismatch strain that was shown to be 4nm thick at the interface by cross-sectional STEM imaging (Supporting Information). Consistent with this loss of crystal ordering, the perpendicular

magnetic anisotropy of the films also becomes very weak. To improve the crystal ordering of $Mn_2Ru_{0.68}Ga$ in the thin film limit, we tested the influence of different seeding layers, including V and TiN, on the growth of $Mn_2Ru_{1-x}Ga$. We found that although the addition of seeding layers on the MgO substrate modulated the strain of $Mn_2Ru_{1-x}Ga$, the magnetic properties were degraded (Supporting Information). We also investigated the effect of substrate annealing on film growth and found substrate annealing prior to the film deposition reduced the coercive field of the thin films (Supporting Information). Based on this extensive study, we conclude that $Mn_2Ru_{1-x}Ga$ films as thin as ~20 nm, which maintains strong perpendicular anisotropy, can be deposited for magnetic free layer applications.

We grew 23 nm $Mn_2Ru_{0.68}Ga$ films to illustrate spin-torque induced switching in this nearly compensated ferrimagnet. From the measured M - H curve (Figure 2(b)), we determined that the saturation magnetization of the film is ~ 30 emu/cm^3 and the out of plane coercivity is around 4 kOe. This saturation magnetization is more than 30 times smaller than regularly utilized ferromagnetic electrode such as CoFeB. The films are then patterned into 4 μm wide Hall bar structures using a combination of photolithography and ion beam etching (**Figure 3(a)**). **Figure 3(b)** shows the anomalous Hall resistance (R_{AH}) as a function of the applied field. To electrically switch the magnetic moment, we apply a series of switching current pulses with 1 ms duration, while applying a static in-plane field (y-axis in Figure 3(a)) of $\pm$ 5 kOe. After each current pulse, a sensing current of 1 mA is utilized to measure the change of R_{AH}. **Figure 3(c)** shows the current-induced spin-orbit torque switching of the device. It can be seen that the current-induced switching has opposite switching polarities under the positive and negative applied constant in-plane fields, which is consistent with the picture of spin-orbit torque induced switching of perpendicularly magnetized films. The magnitude of the static in-plane fields is comparable to those used for Pt/ferromagnet systems

for reaching highest switching efficiency[30]. The role of the in-plane field in spin-orbit torque switching of perpendicular magnetic anisotropy films is to overcome the domain wall chirality due to the Dzyaloshinskii-Moriya interaction (DMI) [30,31]. By applying an in-plane field larger than the effective DMI field, the critical current for switching is minimized. Since the effective DMI field is inversely proportional to the magnetization, the large in-plane fields used in our switching experiments are consistent with the small magnetization. By comparing the results in Figure 3(c) and Figure 3(b), we note that the current-induced switching causes ~50% of the total anomalous Hall resistance change. This is probably due to the wide distribution of electrical current density at the Hall cross location, as the reduced current density at the edge of Hall cross falls below the threshold. The critical current density for switching is ~7.4 × 10^{11} A/m^2, which is similar to those obtained from regular ferromagnetic samples such as Ta/CoFeB/MgO or Pt/Co/AlO_x[26,32], despite of the fact that our film thickness and coercive field are more than 10 times larger than those usually studied films.

We used a harmonic Hall measurement[33,34] to further quantify the spin-orbit torque induced effective magnetic field on the 23 nm $Mn_2Ru_{0.68}Ga$ devices. In this measurement, we applied a low frequency (200 Hz) longitudinal (y-axis in Figure 3(a)) alternating current and measured the in-phase first harmonic $V_{1\omega}$ and out-of-phase second harmonic $V_{2\omega}$ Hall voltages along the x-axis. The $V_{1\omega}$ and $V_{2\omega}$ results under a driving current density of J_e = 1.5 × 10^{11} A/m^2 are shown in **Figure 3(d)** and **Figure 3(e)** as a function of in-plane magnetic field H_y. Using this technique, the effective magnetic fields induced by the damping-like torque and field-like torque H_{DL} and H_{FL} can be determined using the following relationship[33,34]:

$$H_{DL(FL)} = -2\frac{dV_{2\omega}/dH_{y(x)}}{dV_{1\omega}/dH_{y(x)}} \quad (1)$$

Here we can exclude the small contribution from the planar Hall effect and the anomalous Nernst effect because of the small field range probed compared with the anisotropy field and the symmetric and linear second harmonic signals[35]. H_{DL} and H_{FL} extracted using equation (1) for different values of J_e are shown in **Figure 3(f)**. Both H_{DL} and H_{FL} have a linear dependence on J_e, consistent with the origin of spin-orbit torque. Also consistent with spin-orbit torque is the sign dependence of the second harmonic signals for $\pm M_z$ for the dampling-like torque (Figure 3e) and the field-like torque (supporting information). Using H_{DL} we can calculate the effective spin Hall angle through the relation $\xi = \frac{2eM_s t}{\hbar}\frac{H_{DL}}{J_e}$, where $\hbar$ is Planck's constant, e is the charge of an electron, and t is the film thickness. As is summarized in **Figure 3(g)**, the spin Hall angle ξ is determined to be 0.025 ± 0.010, very close to the previously reported numbers in Pt/ferromagnet bilayer systems[26]. This suggests that the spin-torque theory developed for ferromagnetic materials based upon angular momentum conservation holds true for nearly compensated Heusler alloys, which leads to a large effective spin-orbit torque field for samples with diminishing magnetization. The high spin torque efficiency, together with the fact that $Mn_2Ru_{0.68}Ga$ can be switched with reasonably low current densities, indicates that nearly compensated Heusler ferrimagnet can be readily utilized as a free layer for magnetic memory.

To summarize, we studied the magnetic properties of ultrathin Heusler alloy $Mn_2Ru_{1-x}Ga$ films close to the compensation point. Electrically switchable $Mn_2Ru_{1-x}Ga$ thin films that possess strong perpendicular magnetic anisotropy and nearly compensated magnetization are obtained. Current-induced switching with interfacial spin-orbit torque is demonstrated in fabricated Hall bar devices. From harmonic Hall measurements, the spin-orbit torque

efficiency is determined, which is very close to ferromagnetic systems. The fact that a nearly compensated ferrimagnet can be switched as easily as a conventional ferromagnet, in combination with the promising properties of Heusler alloy of high spin polarization, low damping and strong perpendicular anisotropy opens up the possibility of realizing high density, stable, and energy-efficient spintronic devices.

Experimental Section:

We grew $Mn_2Ru_{1-x}Ga$ films at 350 °C by DC magnetron sputtering with a base pressure less than 10^{-8} Torr. We directly sputtered the films on single crystal MgO (001) substrates unless otherwise specified. Following the methods reported in[18], we vary the concentration of the Ru by co-sputtering from Mn_2Ga and Ru targets, where the Mn_2Ga power is kept constant and the Ru power is varied. After the deposition, the films are cooled in vacuum to room temperature and 5 nm Pt or Ru is further deposited on top in-situ. Surface morphology is measured by atomic force microscopy (AFM, Digital Instruments and Asylum Research Cypher) and x-ray diffraction (XRD) is measured with Bruker D8 High Resolution Diffractometer with a Cu-K_α source. Magnetization measurements were carried out using a Digital Measurement Systems vibrating sample magnetometer (VSM). The STEM specimen was prepared using Helios 600i Dual Beam focused ion beam (FIB), using standard lift-out procedure with a final milling step of 1 kV to reduce surface damage. Atomic resolution annular dark field (ADF) STEM images of the Mn_2Ru_1Ga a sample were acquired with an aberration corrected Thermo Themis Z STEM, operated at 300 kV with beam current 20 to 30 pA. The convergence semi angle is 25 mrad and the inner collection semi angles were chosen to range between 75 to 114 mrad to optimize the Z-contrast and signal-to-noise ratio.

Transport measurements are done using a SR810 lock-in amplifier. All measurements are performed at room temperature.

Supporting Information

Supporting Information is available from the Wiley Online Library or from the author.

Acknowledgements

We acknowledge support from Taiwan Semiconductor Manufacturing Company Limited, and National Science foundation under award ECCS-1653553. The material synthesis and characterization were partially supported by the National Science foundation under award DMR 14-19807 through the MRSEC shared facilities. Electron microscopy characterization was conducted in the Frederick Seitz Materials Research Laboratory Central Research Facilities, at UIUC. C. L. and P.Y.H were supported by the Air Force Office of Scientific Research under award number FA9550-7-1-0213.

References:

[1] R. A. de Groot, F. M. Mueller, P. G. van Engen, K. H. J. Buschow, *Phys. Rev. Lett.* **1983**, *50*, 2024.

[2] W. Wang, H. Sukegawa, R. Shan, S. Mitani, K. Inomata, *Appl. Phys. Lett.* **2009**, *95*, 182502.

[3] S. Mizukami, D. Watanabe, M. Oogane, Y. Ando, Y. Miura, M. Shirai, T. Miyazaki, *J. Appl. Phys.* **2009**, *105*, 07D306.

[4] N. Tezuka, N. Ikeda, F. Mitsuhashi, S. Sugimoto, *Appl. Phys. Lett.* **2009**, *94*, 162504.

[5] H. Lin, L. A. Wray, Y. Xia, S. Xu, S. Jia, R. J. Cava, A. Bansil, M. Z. Hasan, *Nat. Mater.* **2010**, *9*, 546.

[6] S. Chadov, X. Qi, J. Kübler, G. H. Fecher, C. Felser, S. C. Zhang, *Nat. Mater.* **2010**, *9*, 541.

[7] H. Kurt, K. Rode, M. Venkatesan, P. Stamenov, J. M. D. Coey, *Phys. Rev. B* **2011**, *83*, 020405.

[8] S. Mizukami, F. Wu, A. Sakuma, J. Walowski, D. Watanabe, T. Kubota, X. Zhang, H. Naganuma, M. Oogane, Y. Ando, T. Miyazaki, *Phys. Rev. Lett.* **2011**, *106*, 117201.

[9] J. Winterlik, S. Chadov, A. Gupta, V. Alijani, T. Gasi, K. Filsinger, B. Balke, G. H. Fecher, C. A. Jenkins, F. Casper, J. Kübler, G.-D. Liu, L. Gao, S. S. P. Parkin, C. Felser, *Adv. Mater.* **2012**, *24*, 6283.

[10] R. Sahoo, L. Wollmann, S. Selle, T. Höche, B. Ernst, A. Kalache, C. Shekhar, N. Kumar, S. Chadov, C. Felser, S. S. P. Parkin, A. K. Nayak, *Adv. Mater.* **2016**, *28*, 8499.

[11] T. Graf, C. Felser, S. S. P. Parkin, *Prog. Solid State Chem.* **2011**, *39*, 1.

[12] I. Galanakis, P. H. Dederichs, N. Papanikolaou, *Phys. Rev. B* **2002**, *66*, 174429.

[13] L. Wollmann, S. Chadov, J. Kübler, C. Felser, *Phys. Rev. B* **2014**, *90*, 214420.

[14] H. van Leuken, R. A. de Groot, *Phys. Rev. Lett.* **1995**, *74*, 1171.

[15] S. Wurmehl, H. C. Kandpal, G. H. Fecher, C. Felser, *J. Phys. Condens. Matter* **2006**, *18*, 6171.

[16] R. Stinshoff, A. K. Nayak, G. H. Fecher, B. Balke, S. Ouardi, Y. Skourski, T. Nakamura, C. Felser, *Phys. Rev. B* **2017**, *95*, 060410.

[17] R. Stinshoff, G. H. Fecher, S. Chadov, A. K. Nayak, B. Balke, S. Ouardi, T. Nakamura, C. Felser, *AIP Adv.* **2017**, *7*, 105009.

[18] H. Kurt, K. Rode, P. Stamenov, M. Venkatesan, Y.-C. Lau, E. Fonda, J. M. D. Coey, *Phys. Rev. Lett.* **2014**, *112*, 027201.

[19] C. Kaiser, A. F. Panchula, S. S. P. Parkin, *Phys. Rev. Lett.* **2005**, *95*, 047202.

[20] Y. Mimura, N. Imamura, Y. Kushiro, *J. Appl. Phys.* **1976**, *47*, 3371.

[21] M. Binder, A. Weber, O. Mosendz, G. Woltersdorf, M. Izquierdo, I. Neudecker, J. R. Dahn, T. D. Hatchard, J.-U. Thiele, C. H. Back, M. R. Scheinfein, *Phys. Rev. B* **2006**, *74*, 134404.

[22] J. Jeong, Y. Ferrante, S. V. Faleev, M. G. Samant, C. Felser, S. S. P. Parkin, *Nat. Commun.* **2016**, *7*, 10276.

[23] K. Borisov, D. Betto, Y.-C. Lau, C. Fowley, A. Titova, N. Thiyagarajah, G. Atcheson, J. Lindner, A. M. Deac, J. M. D. Coey, P. Stamenov, K. Rode, *Appl. Phys. Lett.* **2016**, *108*, 192407.

[24] A. K. Nayak, M. Nicklas, S. Chadov, P. Khuntia, C. Shekhar, A. Kalache, M. Baenitz, Y. Skourski, V. K. Guduru, A. Puri, U. Zeitler, J. M. D. Coey, C. Felser, *Nat. Mater.* **2015**, *14*, 679.

[25] K. Borisov, G. Atcheson, G. D'Arcy, Y.-C. Lau, J. M. D. Coey, K. Rode, *Appl. Phys. Lett.* **2017**, *111*, 102403.

[26] L. Liu, O. J. Lee, T. J. Gudmundsen, D. C. Ralph, R. A. Buhrman, *Phys. Rev. Lett.* **2012**, *109*, 096602.

[27] M. Žic, K. Rode, N. Thiyagarajah, Y.-C. Lau, D. Betto, J. M. D. Coey, S. Sanvito, K. J. O'Shea, C. A. Ferguson, D. A. MacLaren, T. Archer, *Phys. Rev. B* **2016**, *93*, 140202.

[28] D. Betto, N. Thiyagarajah, Y.-C. Lau, C. Piamonteze, M.-A. Arrio, P. Stamenov, J. M. D. Coey, K. Rode, *Phys. Rev. B* **2015**, *91*, 094410.

[29] N. Thiyagarajah, Y.-C. Lau, D. Betto, K. Borisov, J. M. D. Coey, P. Stamenov, K. Rode, *Appl. Phys. Lett.* **2015**, *106*, 122402.

[30] C.-F. Pai, M. Mann, A. J. Tan, G. S. D. Beach, *Phys. Rev. B* **2016**, *93*, 144409.

[31] O. J. Lee, L. Q. Liu, C. F. Pai, Y. Li, H. W. Tseng, P. G. Gowtham, J. P. Park, D. C. Ralph, R. A. Buhrman, *Phys. Rev. B* **2014**, *89*, 024418.

[32] M. Cubukcu, O. Boulle, M. Drouard, K. Garello, C. Onur Avci, I. Mihai Miron, J. Langer, B. Ocker, P. Gambardella, G. Gaudin, *Appl. Phys. Lett.* **2014**, *104*, 042406.

[33] J. Kim, J. Sinha, M. Hayashi, M. Yamanouchi, S. Fukami, T. Suzuki, S. Mitani, H. Ohno, *Nat. Mater.* **2013**, *12*, 240.

[34] U. H. Pi, K. Won Kim, J. Y. Bae, S. C. Lee, Y. J. Cho, K. S. Kim, S. Seo, *Appl. Phys. Lett.* **2010**, *97*, 162507.

[35] K. Garello, I. M. Miron, C. O. Avci, F. Freimuth, Y. Mokrousov, S. Blügel, S. Auffret, O. Boulle, G. Gaudin, P. Gambardella, *Nat. Nanotechnol.* **2013**, *8*, 587.

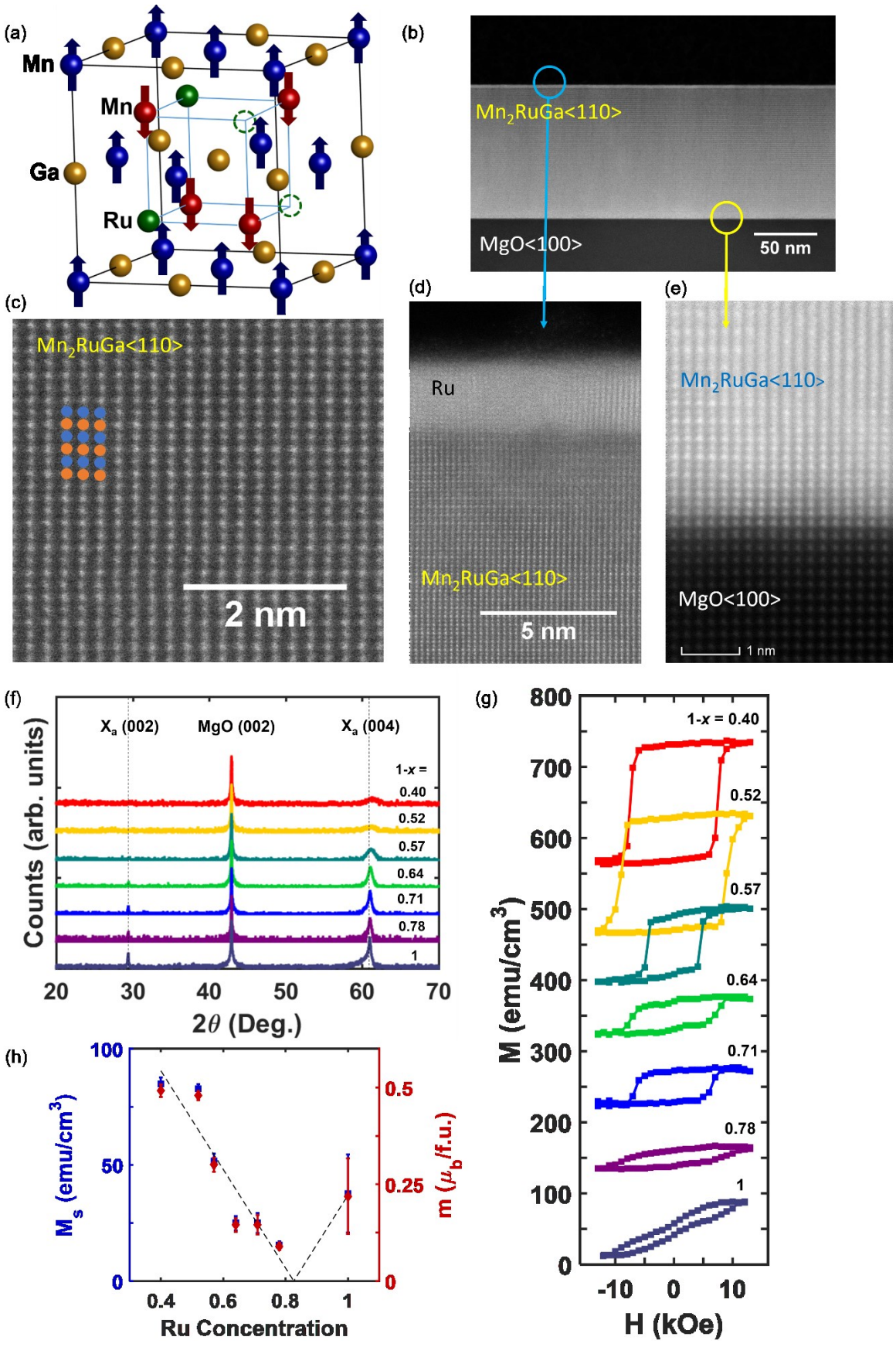

Figure 1. (a) Crystal structure of Heusler alloy $Mn_2Ru_{0.5}Ga$. Note that two different type of Mn atoms occupy the 4a (blue) and 4c (red) sites, separately, while the Ga and Ru atoms take the position of 4b (gold) and 4d (green) sites. Depending on the filling number 1-*x*, there are 0 ~ 4 Ru atoms on 4d sites. The green dashed spheres represent Ru vacancies. (b) STEM image from a 100 nm Mn_2Ru_1Ga sample capped with a 3 nm Ru. (c) Atomic resolution STEM image of Mn_2Ru_1Ga <110> film. The orange and blue circles represent atom layers with and without Ru atoms, where the higher atomic number of Ru causes larger contrast in the dark field image. (d) STEM image of the Mn_2Ru_1Ga/Ru interface that shows low surface roughness. (e) STEM image of the Mn_2Ru_1Ga<110>/MgO<100> interface, showing a clear epitaxial relationship. (f) XRD spectra for 92 nm thick $Mn_2Ru_{1-x}Ga$ films with varying Ru concentration 1-*x*. (g) Magnetic hysteresis loops for the series of films measured by VSM. (h) Saturation magnetization M_s and magnetic moment (in units of Bohr magneton μ_B) per formula unit m as a function of Ru concentration. The dashed line serves as a guide for eye. The point with zero magnetic moment is determined with the assistance of an anomalous Hall effect measurement, which is shown in the supporting information.

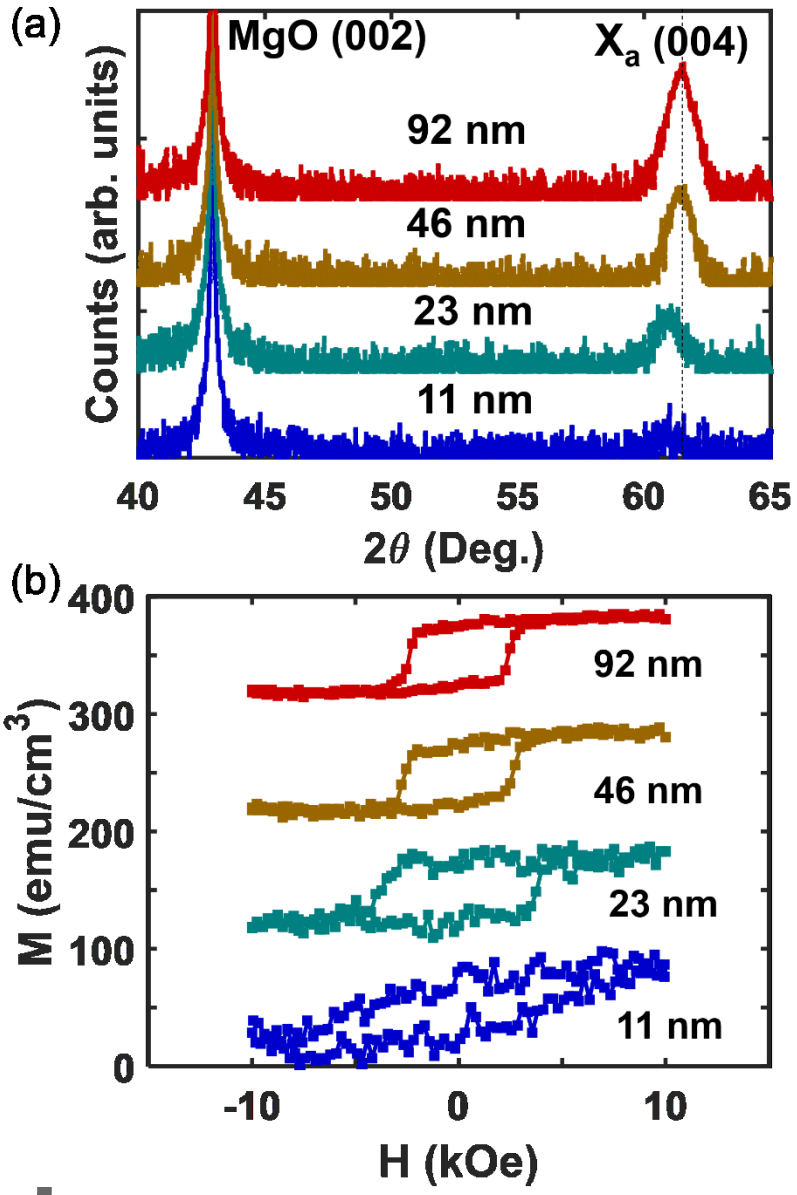

Figure 2. (a) XRD spectra for $Mn_2Ru_{0.68}Ga$ films with different thickness. (b) Magnetic hysteresis loops of $Mn_2Ru_{0.68}Ga$ films as a function of thickness.

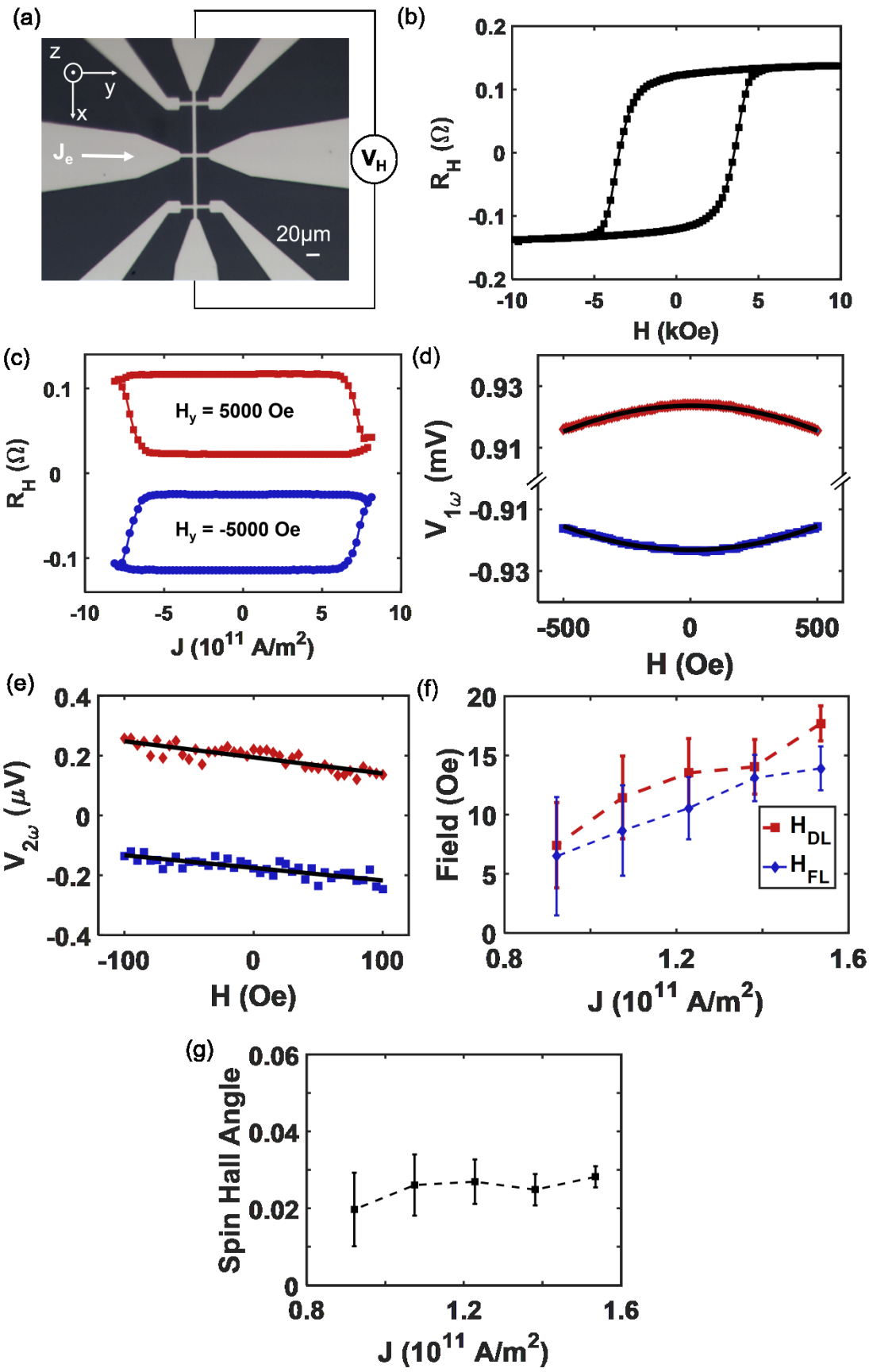

Figure 3. (a) Microscope image of a Hall bar structure of $Mn_2Ru_{0.68}Ga$ (23 nm)/Pt (5 nm) showing the geometry of applied current J_e and measured Hall voltage V_H (b) Anomalous Hall resistance R_H as a function of applied magnetic field for the sample in (a). (c) Spin-orbit torque induced switching with applied in-plane fields of 5 kOe and -5 kOe. Switching data are offset for visibility. (d) First harmonic voltage $V_{1\omega}$ *vs* H_y for magnetic moment aligned around the positive (red) and negative (blue) equilibrium positions near the z-axis. The field direction is defined by the coordinate system illustrated in (a). The applied current density for this measurement is J_e = 1.5×10^{11} A/m^2 . (e) Second harmonic voltage $V_{2\omega}$ vs H_y with J_e = 1.5×10^{11} A/m^2. (f) Effective fields caused by damping-like H_{DL} and field-like H_{FL} torques as a function of applied current densities. (g) Calculated spin Hall angle of Pt as a function of applied current densities.

The epitaxial growth of Ferrimagnetic Heusler thin films is reported, with magnetic properties optimized based upon concentration and thickness. Efficient current-induced magnetic switching is demonstrated for a nearly compensated ferrimagnet that has a relatively large thickness and robust stability, opening the door for the possible use of compensated ferrimagnets for fast, energy-efficient spintronic devices.